ZnO nanostructures based innovative photocatalytic road for air purification

Marie Le Pivert, Olivier Kerivel, Brahim Zerelli, Yamin Leprince-Wang

Version of Record: https://www.sciencedirect.com/science/article/pii/S0959652621026597
Manuscript_b5e90768a28bed61a10d7bcd270304a0

ZnO Nanostructures based innovative photocatalytic road for air purification

Marie Le Pivert[a,b], Olivier Kerivel[a], Brahim Zerelli[a], Yamin Leprince-Wang[a]*

[a]ESYCOM, Univ Gustave Eiffel, CNRS (UMR 9007), F-77454 Marne-la-Vallée, France

[b]COSYS-LISIS, Univ Gustave Eiffel, IFSTTAR, F-77447 Marne-la-Vallée, France

* Corresponding author: Yamin Leprince-Wang (yamin.leprince@univ-eiffel.fr)

Abstract:

Atmospheric pollution is a major issue affecting environment and health. Therefore, semi-conductor-nanoparticles-based photocatalytic infrastructures appeared as a promising solution to improve urban air quality due to their abilities to mineralize toxic organic compounds. To avoid the direct use of free nanoparticles, as nanomaterials are suspected to be carcinogenic, this work intends to develop civil engineering materials functionalized by direct growth of ZnO nanostructures as a more environmentally friendly and biocompatible approach to reduce the air pollution. By scaling-up an innovative and low-cost hydrothermal direct growth synthesis, a few square meters paved with tiling and bitumen road were easily produced in order to evaluate their photocatalytic activity at large scale under solar lamp in a climatic chamber (Sense-City, 3200 m^3) to reflect real atmospheric air purification situations. Observations provide insights into their ability to simultaneously remove various pollutants from a real car exhaust (O_3, CO_X, NO_X, VOCs) and their durability, as well as understandings of the weather conditions impact on the photocatalytic degradation of these pollutants and of the relationships between pollutants trend evolution. This study also seems to prove that, when exposed to sunlight, bitumen roads are responsible of pollutants emission and causes modifications in the Chapman cycle.

Keywords: Air purification, Innovative Road, Photocatalysis, Advanced oxidation process, Zinc Oxide Nanostructures, Climatic chamber.

1. Introduction

To address issues of outdoor air pollution, which caused 4.2 million premature deaths worldwide in 2016 as estimated by World Health Organization (WHO), photocatalytic infrastructures were rapidly developed since past decades to improve urban air quality, due to their abilities to degrade and mineralize toxic organic pollutants into harmless compounds as H_2O, CO_2, NO_3^- (Senff et al., 2014; Singh et al., 2018). Their use as paving blocks in public roads or as motorway sound barriers were imposed by the need to be in the direct road environment (Hüsken et al., 2009), in order to ensure their exposure both to light and to pollutant molecules. To this end, photocatalyst integration in a mixture with concrete, cement, and paint (Senff et al., 2014; Singh et al., 2018; Cerro-Prada et al., 2018) or as free mediate in a surface layer (Guo et al., 2017; Nath et al., 2016; Darvish et al., 2020) were employed to produce depolluting surface. For both strategies, the most commonly used photocatalyst was titanium dioxide, under the form of nanoparticles. Nevertheless, it now suffers from a lack of popularity caused by the TiO_2 nanoparticles (TiO_2 NPs) possible carcinogenic effect (Grande and Tucci, 2016; Dar et al., 2020). Therefore, it is imperative to develop new photocatalytic surfaces using other photocatalysts that can remove complex hazardous pollutants from air, and thus to study their efficiency at a real scale with complex pollutants sources.

In that way, efforts were made to replace TiO_2 by other photocatalysts, such as zinc oxide (ZnO). ZnO is indeed well known for its high photocatalytic activity (Liu et al., 2019; Shinde et al., 2017; Pastor et al., 2019), its good chemical stability, its non-toxicity (Li et al.,

2008) and its low cost for both raw materials and nanostructure synthesis by hydrothermal method. Moreover, the hydrothermal route has already proven its easiness and its efficiency to synthesize ZnO nanostructures (ZnO NSs) onto non-conventional substrates as stainless-steel mesh film (Wang et al., 2012), flexible PDMS (Zhang et al., 2019), polyester fibbers and other ceramics (Danwittayakul et al., 2013).

Recently, it was also proved that the hydrothermal synthesis could be used to implement ZnO NSs onto the surface of commercially available construction materials, such as concrete and tiling, thus avoiding waste by a non-embedding photocatalyst surface in the materials and providing excellent photocatalytic activity at laboratory scale (M. Le Pivert et al., 2019, 2020). In addition, it was assumed that this direct growth onto civil engineering materials could improve ZnO NSs resistance to abrasion and weathering, leading to reduced risks of release in the environment. Besides, the hydrothermal synthesis is easy to upscale in order to produce huge surfaces for daily life outdoor civil engineering materials.

Despite excellent results at laboratory scale, these depolluting surfaces suffer from a lack of knowledge on their efficiency for air depollution test at large scale. In fact, data obtained from laboratory scale tests are not really suitable for extrapolating scale-up test results. Photocatalysis is indeed very sensitive to experimental conditions, thus justifying disparities between real scale and laboratory scale experiments (Maggos et al., 2007; Chen and Chu, 2011). Hence, evaluating their efficiency under near real atmospheric conditions and different weathers, with strict climatic conditions control is a crucial step for their development, but implies the use of a relevant large and enclosed space, where different climatic factors such as temperature, humidity, solar light intensity, and pollutant concentration could be controlled. For those reasons, the Sense-City climatic chamber, with its surface of 400 m^2 and volume of 3200 m^3 (Gustave Eiffel University, France) (Sense-City

Website, 2021), covering a town reproduction equipped with houses, roads, sunlight simulator, temperature and humidity controller, numerous gas sensors, and high performant gas analyser for ozone (O_3), nitric oxides (NO_X), volatile organic compounds (VOCs) and carbon oxides (CO_X) concentration measurements, offers perfect conditions for photocatalytic road evaluation.

The main novelty of this study is therefore to implement ZnO on building construction materials by a direct hydrothermal growth at mid-scale, and to evaluate its efficiency at large scale with a real pollution source. Here, to perform this study, a mid-scale hydrothermal synthesis was developed as a way to functionalize a relevant quantity of tilings and rock aggregates by direct growth of ZnO nanowires (NWs) on these surfaces. Tilings and rocks aggregates were then used for creating two kinds of photocatalytic road infrastructures: (1) tiling pavement surfaces, to simulate either motorway sound barriers or pavement on public roads (3 panels, each one measuring about 0.63 m^2); and (2) a bitumen road surface (2 squares, each one measuring 1 m^2), thanks to a simple integration of functionalized rock aggregates in cold bitumen without needing to modify existing road infrastructures. Then, those depolluting surfaces were evaluated for photocatalytic degradation of real car exhaust gas at relevant scale with different configurations and weather conditions in the Sense-City climatic chamber. The obtained results demonstrated the good quality of ZnO NWs directly synthetized on photocatalytic road infrastructures, their performances to remove simultaneously O_3, NO_X, VOCs and CO_X from petrol car exhaust at mid-scale, and the influence of road type and weather conditions, such as temperature, humidity, airflow (wind), on photocatalytic efficiency.

2. Material and Methods

2.1 Depolluting surface production

Commercially available tiling (14.5 x 14.5 x 0.6 cm tiling purchased from DIY retailer Leroy Merlin, France) and mineral rock aggregates (Quartzite rock aggregates 4-6 mm supplied by EIFFAGE, France) were used as substrates for the innovative road covered by ZnO nanostructures production. Figure 1 schematically summarizes the depolluting road infrastructures production process in three main steps: 1) ZnO seed layer creation by a "horizontal impregnation" method followed by an annealing, 2) ZnO direct hydrothermal growth, 3) functionalized civil engineering material integration as road infrastructures.

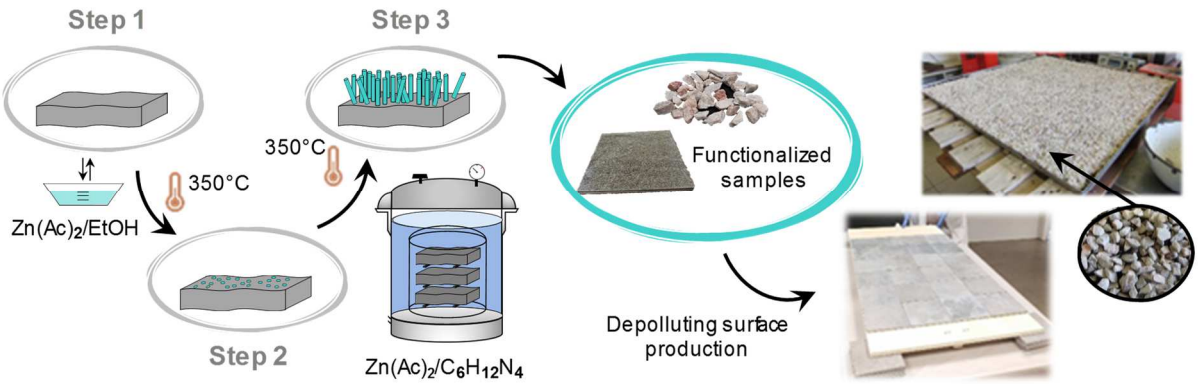

Figure 1. Depolluting road infrastructures production.

Both substrates were firstly rinsed, dried, and prepared by a "horizontal impregnation" method followed by an annealing in order to create a nucleation ZnO seed layer, as described in our previous work (M. Le Pivert et al., 2019, 2020). On the contrary to tiling surface, where only the top surface was impregnated by the seed layer solution, rock aggregates were totally immerged in this solution, which allowed a possible growth on the entire surface of rock aggregates.

Secondly, a scaled-up classical hydrothermal synthesis in an autoclave containing 8 L of an aqueous solution of hexamethylenetetramine (HMTA, ≥ 99%, VWR, CAS-No 100-97-0) and zinc acetate dihydrate ($Zn(Ac)_2 \cdot 2\ H_2O$, 98%, Sigma-Aldrich, CAS-No 5970-45-6) at 0.025 M was carried out at 90°C for 2h. Then, the samples were annealed 30 minutes at 350°C and thoroughly characterized by UV-visible spectroscopy (Maya2000 Pro, Ocean Optics) and field-emission scanning electron microscopy (Zeiss FE-SEM NEON 40). To make SEM observations possible and easier, three tiling samples were broken in small part using a hammer and a screwdriver.

Functionalized tilings were then fixed onto a wood board thanks to a commercial resin in order to represent a paved roadway or a motorway noise barrier (wall). Functionalized mineral rock aggregates were then integrated as a monolayer in a cold bitumen emulsion, with the help of the company EIFFAGE France, to mime a roadway surface. Three functionalized tiling panels of 0.63 m^2 and 2 x 1 m^2 of functionalized bitumen road were produced.

2.2 Road traffic purification by photocatalysis in the Climatic chamber Sense-City

Sense-city (UGE) is a climatic chamber at Champs-sur-Marne that can cover two portions of territory of 400 m^2. These portions represent a small town (Mini-Ville) with urban infrastructures as house and road, which, once covered, represents a closed volume of 3200 m^3. In this closed and airtight space, air, water, and soil pollution can be monitored, thanks to numerous fixed sensors and mobile high performance gas analysers. Temperature, humidity, as well as sunlight, can be monitored and controlled in Sense-City.

Thus, thanks to this equipment, different measurement campaigns were carried out in the Mini-Ville 1 (Figure 2(a)), where different relative humidity and room temperatures were

logged with the aim to study the climatic influence on the photocatalytic efficiency of innovative road infrastructures. Different weathers conditions (temperature (T°C) and relative humidity (RH) (%)) were tested: (1) 30°C and 45%; (2) 20°C and 55%; (3) 20°C and 50 %; (4) 20°C and 35%; (5) 30°C and 30%. Three kinds of photocatalytic road infrastructures dispositions were also studied, as shown in Figure 2: (b) two tiling walls and one bitumen road; (c) three tiling walls and two bitumen roads; (d) three tiling walls disposed as paved road. In order to monitor pollutants, gas analysers (AC32M, CO12e, O342M; Environmental S.A.) were used and their sensing ends were placed just above the road surface. Then, the analyser's sensing ends were placed at 50 cm above the road surface in order to know if the depollution could be measured far away from the surface (Figure 2(e)). A VOCs sensor (EcologicSense, AQ Sense - e-VOC industry) was also used, with a fixed placement at ~ 1 m 10 from the soil (in the suspended box near the gas analysers) (Figure 2(c)).

To each condition exposed above, an experimental scenario was applied to create, stabilise and follow the car exhaust gas concentration changes over time. This experimental scenario is divided in 5 phases: (1-2) pollution creation thanks acceleration and lets turn on petrol car; (3) pollution stabilisation in the climatic chamber after turning off the car; (4) adsorption in the dark on the ZnO nanostructures; (5) photocatalysis under artificial solar light ($UV_{290\text{-}390\ nm} \geq 1900 – 2530\ \mu W/cm^2$) (Figure 2(f)). A scenario similar to the one presented in Figure 2(f) with ZnO surfaces covered during the entire scenario was used as a reference to study the natural pollutants evolution in the climatic chamber. Then, the duration of phases 2, 3 and 4 was reduced from 30 min to 15 min between the beginning and the end of the campaign, without any modification of the other following phases and without any problems for result reproducibility and comparison.

Thanks to the gas analysers, ozone, nitric oxide, nitrogen dioxide, carbon monoxide and carbon dioxide were followed in real time with a measurement every 2 minutes. Considering that only the results from the photolysis and photocatalysis (phase 5) showed some variations and differences between ZnO and reference, only phase 5 results will be presented and analysed in this work. The measured concentrations were converted in relative evolution, using Equations (1) and (2) to express a diminution rate X(%) and a formation rate Y(%) during the photocatalysis phase.

$$X(\%) = \frac{C}{C_0} \times 100 \quad (1)$$

$$Y(\%) = \frac{C - C_0}{C_0} \times 100 \quad (2)$$

Where C_0 and C stand for the initial and actual concentration values during the studied photocatalysis phase, respectively, for the understudied pollutant. O_3 concentration stayed under 10 ppb; CO concentration was between 0 and 2 ppm except during the pollution creation phase, were values up to 4 could be obtained; CO_2 concentration was between 800 ppm and 1200 ppm except during the pollution creation phase, were values up to 1400 could be measured; NO concentration was between 40 and 120 ppb except during the pollution phase, where higher concentrations could be recorded; finally, NO_X concentration was between 50 and 100 ppb except during the pollution phase, where higher concentrations could be registered.

Equation (3) was used to evaluate the medium difference between results from identical scenarios.

$$medium\ difference = \frac{1}{n} \sum |x - \overline{x}| \quad (3)$$

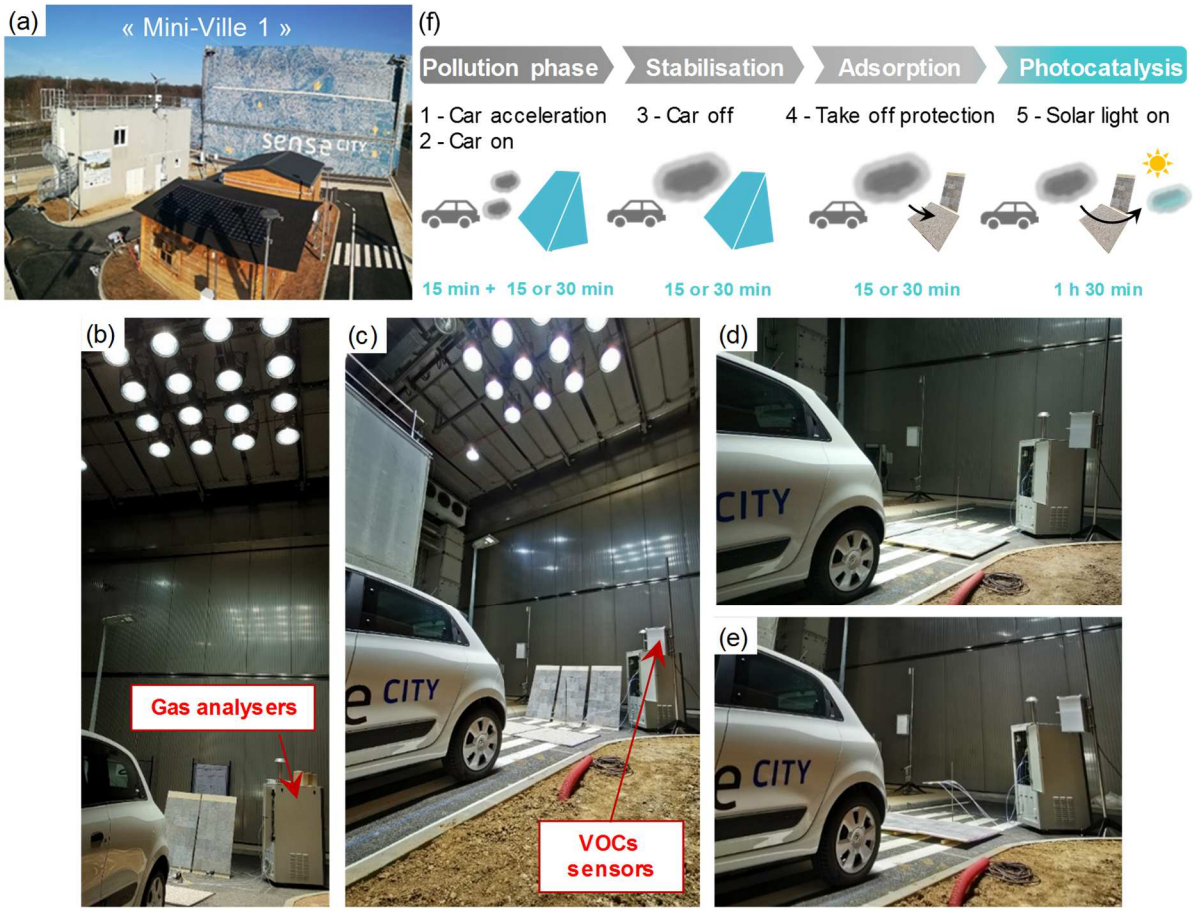

Figure 2. Sense-city experimental campaign pictures **(a-e)** and schematic experimental scenario applied **(f)**.

3. Results and discussions

3.1 Depolluting road infrastructures characterisation

The morphologies of ZnO nanostructures grown on construction materials by hydrothermal process were characterized by scanning electron microscopy (SEM). Despite a violent cleavage method (see material and methods section), ZnO NWs observed by top and cross-section views still seem well aligned with no apparent damage (Figure 3(a)). It suggests the good efficiency of hydrothermal synthesis to strongly fix the ZnO nanostructures onto civil engineering materials by direct growth on it, no matter the placement of samples during synthesis. In fact, the tiling samples were synthesized three at the same time, by placing

three samples in a three-stage support inside the chemical bath (Figure 1). An average diameter of 54 nm ± 6 nm and an average length of 1.7 µm ± 0.2 µm were measured for all tiling samples. Those results are very similar with our previous work, where the samples were synthesized individually in small size (M. Le Pivert et al., 2019, 2020), reflecting on the one hand the scale-up process success; and on the other hand, the good homogeneity of ZnO NWs on each tiling samples. No apparent changes in ZnO NWs morphology were observed on rock aggregate samples (Figure 3(b)). Nevertheless, due to the non-plane and very chaotic surface state as well as the complex chemical composition of the construction material substrate, hindered surface and possible turbulence lead to a local heterogeneity in the nanostructure growth, leading to ZnO NWs oriented in various and random way with punctually larger or smaller NWs as mentioned in our previous work (M. Le Pivert et al., 2019, 2020). An average diameter of 73 nm ± 9 nm was measured. No cross-section was possible for those samples, but considering the morphology obtained from plan view observation, it can be assumed that the ZnO nanostructure dimensions are close to the ones of the tiling samples.

Then, UV-Visible spectroscopy has been employed for gap measurement. The Tauc-Lorentz relation (Equation (4)) was applied to the absorption spectra obtained.

$$\alpha h\nu = A(h\nu - E_{gap})^m \quad (4)$$

Where α is the adsorption coefficient, ν is the frequency of light, h is the Plank constant, A is a constant, E_{gap} is the bandgap and m depends on the type of bandgap transition (direct or indirect, allowed or unallowed). It is well known that ZnO is a direct-bandgap and thus m is equal to 1/2. Therefore, the plot of the absorption spectra leads to a liner part $\alpha h\nu = A(h\nu - E_{gap})^2$. The intercept of a straight line on this linear part with the hν axis is the bandgap.

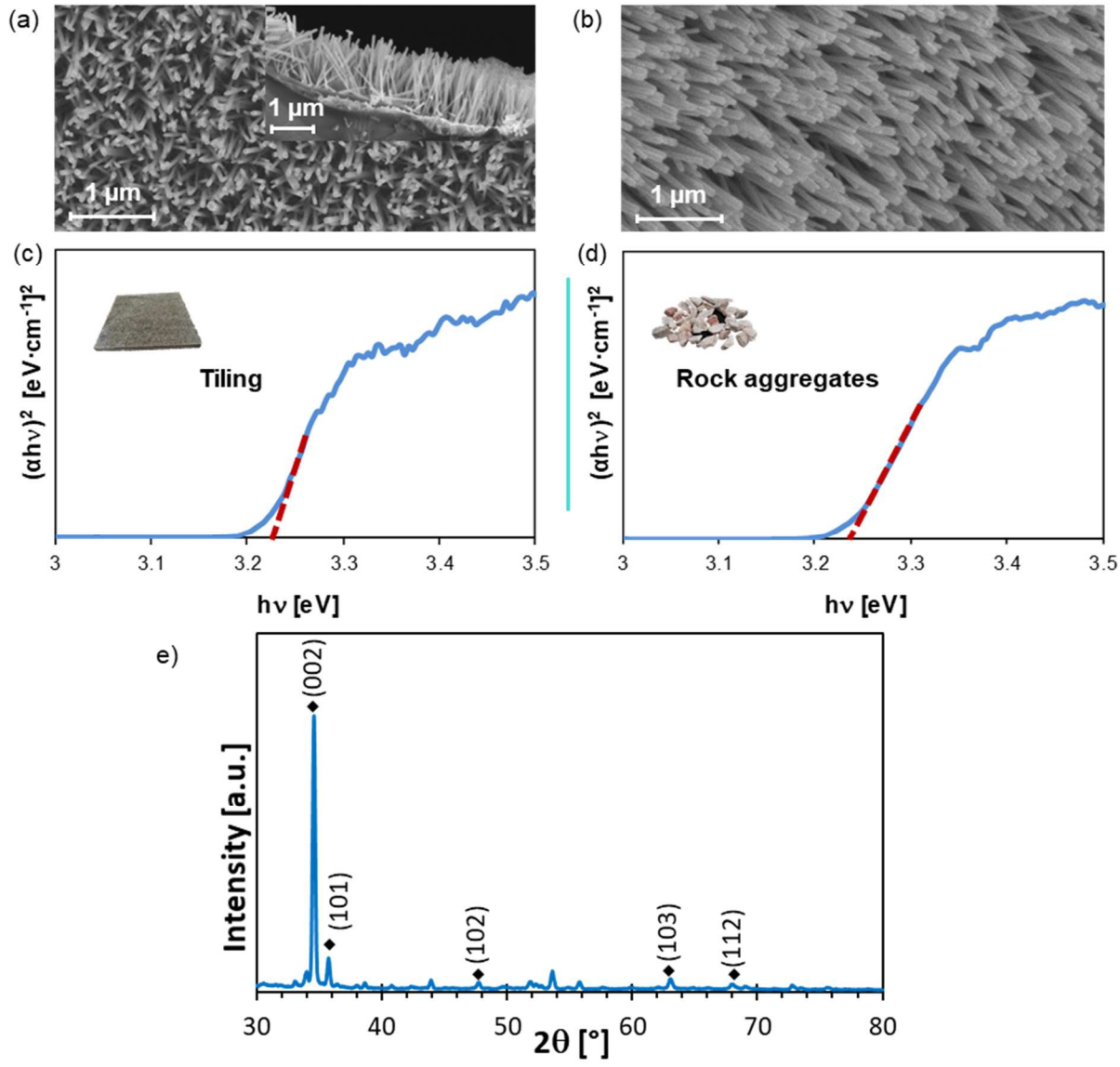

Figure 3. Depolluting road infrastructures characterization (SEM images of ZnO NWs onto tiling **(a)** and rock aggregate **(b);** UV-visible absorbance spectral plot with the Tauc-Lorentz model of ZnO NWs onto tiling **(c)** and rock aggregate **(d)**; XRD pattern of ZnO nanowires grown on tiling surface).

To obtain a representative value and to check the reproducibility of the synthesis method, measurements were carried out on each tiling sample and on six rock aggregates randomly chosen after each synthesis (about ~ 650 g). For each sample, different measurements were taken from different positions in order to check the good homogeneity

and quality of the ZnO nanostructures synthesized onto these non-conventional substrates. Tauc-Lorentz plots of UV-Vis absorbance spectrum of ZnO (Figures 3(c,d)) reveal an average gap value of 3.23 eV ± 0.02 eV and 3.22 eV ± 0.02 eV for tilings and rock aggregates samples, respectively. As can be seen from Figure 3(e), the X-ray diffraction (XRD) spectrum (CuKα, λ = 1.5418 Å) of ZnO grown onto tiling showing a hexagonal Wurtzite structure. XRD pattern of ZnO NWs grown on different substrate comparison demonstrated that there is no differences between ZnO nanowires grown on silicon and on tiling (C. Chevalier-César et al., 2014). It is therefore possible to assume that ZnO nanowires on tiling and rock aggregate have the same or very close quality to those grown on silicon substrate. In agreement with our previous work (M. Le Pivert et al., 2019), the adapted hydrothermal method once again demonstrated its ability to generate highly homogeneous ZnO NWs with high qualities on different kind of chaotic substrate. That means this innovative adapted method is suitable for the direct growth of ZnO nanostructures on construction materials, allowing a scale-up synthesis for industrial application.

3.2 Air purification by photocatalysis under solar light in Sense-City

As described above and in the materials and methods section, Sense-city is a mobile climatic chamber, which can cover a town reconstitution equipped with several gas analysers, sunlight simulator and weather controller (Figure 2(a)). Therefore, after producing tiling walls and bitumen road functionalized by ZnO NWs (Figure 1), their efficiency in depolluting the car exhaust gas was studied in the climatic chamber Sense-City under different weather conditions and infrastructure configurations (Figures 2(b-e)). An experimental scenario was applied in order to create, stabilise and follow the car exhaust gas concentration changes over time (see materials and methods section, Figure 2(f), only results from the photocatalytic phase will be discussed (Figure 2 (f)).

3.2.1 Evaluation of photocatalytic infrastructures efficiency

3.2.1.1 Results

Reference (without ZnO) results showed a natural formation of toxic and hazardous O_3 contaminant under solar light (Figure 4(a)). A possible formation mechanism related with VOCs oxidation (Figure 4(b)) will be discussed in the following section. A similar natural trend of O_3 formation was observed for CO evolution under solar light (Figure 4(c)). Conversely, a natural dilution of CO_2, NO and NO_x appeared during the reference in the climatic chamber due to its large dimensions and their adsorption by the surfaces inside the climatic chamber (Figures 4(d-f)).

With the use of photocatalytic road infrastructures, O_3 and CO emissions under solar light are strongly reduced, and CO_2, NO and NO_x concentrations decrease more rapidly (Figures 4(a-f)). After 90 min under solar light irradiation in presence of ZnO NS, the O_3 emission was divided by two (57% with ZnO against 125% without). Under the same conditions, the CO emission was divided by more than 4 (11% with ZnO against 53% without). A very narrow difference of 1% on CO_2 reduction was recorded (97% with ZnO against 98% without). NO and NOx residue rates were also reduced by the presence of ZnO Ns, with a diminution of 5% and 4% respectively (81% with ZnO against 86% without, and 97% with ZnO against 91%). The error bars represent the gap average between two tests realized with ZnO photocatalytic road infrastructures. The difference between both tests could be also due to slight variations of temperature, humidity and initial pollutant concentration produced by a manual acceleration of the car with a fixed duration. Nevertheless, the different measurements showed relatively reproducible results and no loss of photocatalytic efficiency of the ZnO-nanostructures-functionalized surfaces over

time. These results are very convenient for their applications as outdoor infrastructures to deal with the air pollution produced by road traffic. At 30°C and RH = 45%, photocatalytic road infrastructures in configuration 1 (Figure 2(b)) demonstrated a promising efficiency for real car exhaust gas depollution at large scale.

Despite the impossibility to make direct comparison with previous results due to the non-identical experimental conditions, it is important to put results into perspective. Concrete road modified by TiO_2 NPs demonstrated a decontamination rate for NOx between 14% and 16% (2 – 6.5 mol/m^3) in outdoor experiments, depending on the weather conditions (Chen and Chu, 2011). Photocatalytic TiO_2 coating layer for asphalt pavement (10 cm × 15 cm × 1 cm) in a testing chamber under UV Xenon Lamp (300-400 nm, 304 W/m^2) with 1 ppm of NO (1L/min) and a RH of 50-60% at 25-30°C led to a decontamination of 38% and 10% before and after road polishing (Wang et al., 2017). g-C_3N_4/$BiVO_4$ powder composite in a testing chamber (680 mm × 530 mm × 530 mm) under visible light (400-780 nm, 4 W) led after 10 min to a decomposition rate of CO and NO between 2.5% and 6% and 17.5% and 27% depending on the mass ratio of g-C_3N_4/$BiVO_4$ (Cui et al., 2020). 20 mg of Bi/$Bi_2O_2CO_3$ on Bi_2WO_6 nanosheets in a quartz reactor containing 3000 ppm of chlorobenzene at RH ~ 45% and T ~ 25°C, which is a VOC, led to a removal efficiency of 97% after 5 hours under a 300 W Xe-lamp (Liu et al., 2018). The Sense-city dimensions could explain the smaller decontamination rates obtained as they reduce the probability of pollutant adsorption on photocatalyst. The competition of the pollutants for OH radicals and for adsorption sites on the catalyst surface could also justify the different results (Chen and Chu, 2011).

3.2.1.2 Photodegradation synergistic mechanism proposition

The natural emission of O_3 under solar light with and without ZnO Ns may be related to the significant VOCs presence, as they are emitted by the petrol car during the pollution phase emissions and produced by the bitumen road under solar light irradiation and heating; as well as their oxidation. Oxidative VOCs can replace O_3 for the NO reduction in the Chapman cycle and thus conduct to increase the O_3 concentration under solar light (Figure 4(b)). O_3 formation could therefore be assigned to a modification of the Chapman cycle by the car pollution. A natural trend, similar to O_3 formation, was observed for CO evolution under solar light (Figure 4(c)). This natural formation could also be attributed to VOCs from car exhaust and bitumen road presence. In fact, VOCs, as Hydrocarbons, could react under solar light or with O_3 and NO, leading to CO emission.

With the use of photocatalytic road infrastructures, O_3 and CO emissions under solar light are strongly reduced (Figures 4(a, c)). The decreasing O_3 formation rate could be explained by a photocatalytic degradation of VOCs by the ZnO-nanostructure-functionalized road infrastructures and thus by a reduction of the Chapman cycle modification. On the other hand, O_3 direct photodegradation over ZnO nanostructures could also explain this trend (equations (5) to (15)). Indeed, O_3 could react with photo-generated electrons or with superoxide ions from the reduction of O_2, leading to other oxidant radical species able to generate O_2 or hydroxyl radical ($OH^{\bullet}$). Moreover, these equations reveal a synergic effect between O_3 and the photocatalytic process leading to higher $OH^{\bullet}$ formation thanks to a stronger electron affinity of O_3 compared to the electron affinity of O_2 (Da Costa Filho et al., 2019). Therefore, the direct photocatalytic degradation of O_3 could help the VOCs photocatalytic degradation onto ZnO, leading to a reduction of the natural O_3 formation under solar light. Consequently, the O_3 photocatalytic reduction observed above could explain why CO follows the same trend in the presence of ZnO-nanostructures-covered road

surfaces. Besides, CO diminution could also be due to Hydrocarbons and CO photocatalytic degradation and conversion into CO_2 (Bayjoo et al., 2017).

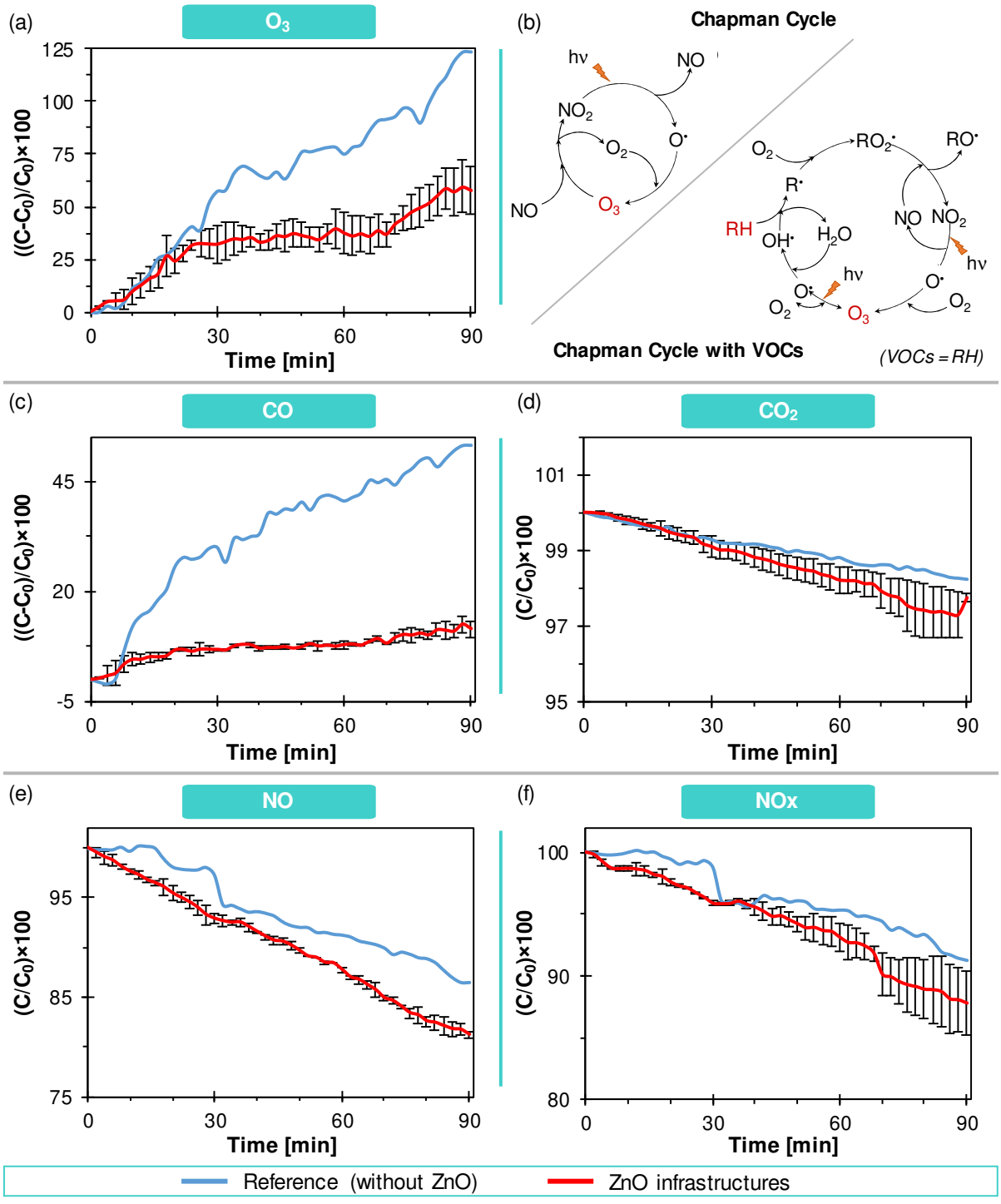

Figure 4. Pollutant evolution under solar light with and without ZnO (Plots of pollutant concentration evolution as function of photocatalysis time under artificial solar light with

and without the presence of ZnO at 30°C and RH = 45% in Sense-City **(a, c-f)**; Schema of natural and modified Chapman cycle **(b)**).

Nevertheless, no CO_2 emission was recorded in the presence of ZnO (Figure 4(d)). A slight diminution of CO_2 is even observed and could be due to some adsorption phenomenon with free active site liberation on ZnO surface after the photocatalytic degradation of other pollutants. CO_2 could also be oxidized by hydroxyl radicals and converted into CO_3^{2-} (Cui et al., 2020). These results suggest a good photocatalytic efficiency of innovative road infrastructures.

$$ZnO + h\nu \rightarrow e_{CB}^{-} + h_{VB}^{+} \quad (5)$$

$$O_3 + e_{CB}^{-} \rightarrow O_3^{\bullet -} \quad (6)$$

$$O_3^{\bullet -} + H^{+} \rightarrow HO_3^{\bullet} \quad (7)$$

$$HO_3^{\bullet} \rightarrow O_2 + OH^{\bullet} \quad (8)$$

$$O_3 + O_2^{\bullet -} \rightarrow O_3^{\bullet -} + O_2 \quad (9)$$

$$O_3 + 2\,O_2^{\bullet -} + H_2O \rightarrow 2\,O_2 + OH^{-} + OH^{\bullet} \quad (10)$$

$$O_3 + OH^{\bullet} \rightarrow HOO^{\bullet} + O_2 \quad (11)$$

$$O_3 + OH^{\bullet} \rightarrow O_4^{\bullet -} + H^{+} \quad (12)$$

$$O_3 + O_3^{\bullet -} \rightarrow O_4^{\bullet -} + O_2 \quad (13)$$

$$O_3 + O_4^{\bullet -} \rightarrow O_3^{\bullet -} + 2\,O_2 \quad (14)$$

$$O_3^{\bullet -} + O_4^{\bullet -} + H^{+} \rightarrow 3\,O_2 + OH^{-} \quad (15)$$

Good photocatalytic performances were also recorded for NO removal with a strong reduction of NO, using photocatalytic road infrastructures under artificial solar light. A

similar trend was observed for NO_X removal. Figures 4(e) and 4(f) reveal more errors on the NO_X average curve than on the one of NO. In fact, the participation of NO_2, which is a by-product of NO before its conversion into HNO_2, HNO_3 or NO_3^- (equations (16) to (25)) (Kowsari and Bazri, 2014; Todorova et al., 2015; He et al., 2017; Mahy et al., 2019), could explain why less reproducible results are obtained on NO_X. Moreover, as can be seen in equations (19) and (20), there is an equilibrium between NO_2 and HNO_2 production. The degradation pathway could be summarized by the conversion of NO into HNO_3 or NO_3^- by photo-oxidation via NO → HNO_2 → NO_2 → HNO_3 or NO_3^- (Bayjoo, et al. 2017; Staub de Melo and Trichês, 2012).

$$NO + h^+ \rightarrow NO_2 + H^+ \quad (16)$$

$$2\,NO + O_2^{\bullet -} + 3e^- \rightarrow 2\,NO_2 \quad (17)$$

$$NO + OH^\bullet \rightarrow NO_2 + H^* \quad (18)$$

$$NO + h^+ + H_2O \rightarrow HNO_2 + H^+ \quad (19)$$

$$HNO_2 + OH^\bullet \rightarrow NO_2 + H_2O \quad (20)$$

$$NO_2 + OH^\bullet \rightarrow HNO_3 \quad (21)$$

$$NO + h^+ + H_2O + {}^1/_2\,O_2 \rightarrow HNO_3 + H^+ \quad (22)$$

$$NO + O_2^{\bullet -} \rightarrow NO_3^- \quad (23)$$

$$NO_3^- + NO + h^+ \rightarrow 2\,NO_2 \quad (24)$$

$$3\,NO + 2\,OH^- \rightarrow 2\,NO_3^- + NO + H_2O \quad (25)$$

The proved ability of photocatalysis to remove simultaneously various pollutants makes this process a very competitive air treatment method, able to depollute O_3, CO_X, NO_X at the same time with a synergic effect between pollutants degradation.

3.2.2 Climatic conditions influence onto photocatalytic infrastructure efficiency

It is well-known that the meteorological conditions, like humidity and temperature, have a powerful impact on the photocatalytic efficiency (Guo et al., 2017; Chen and Chu, 2011; Staub de Melo and Trichês, 2012). For this reason, new experimental conditions were logged: 20°C ± 2°C (room temperature) and 55% ± 3 % (RH). ZnO-nanostructure-functionalized infrastructures remained in configuration 1 (Figure 2(b)) in order to be compared to results obtained at T = 30°C ± 2°C and RH = 45% ± 2%. Only O_3 and NO will be discussed in this part due to their correlation with other pollutants evolution.

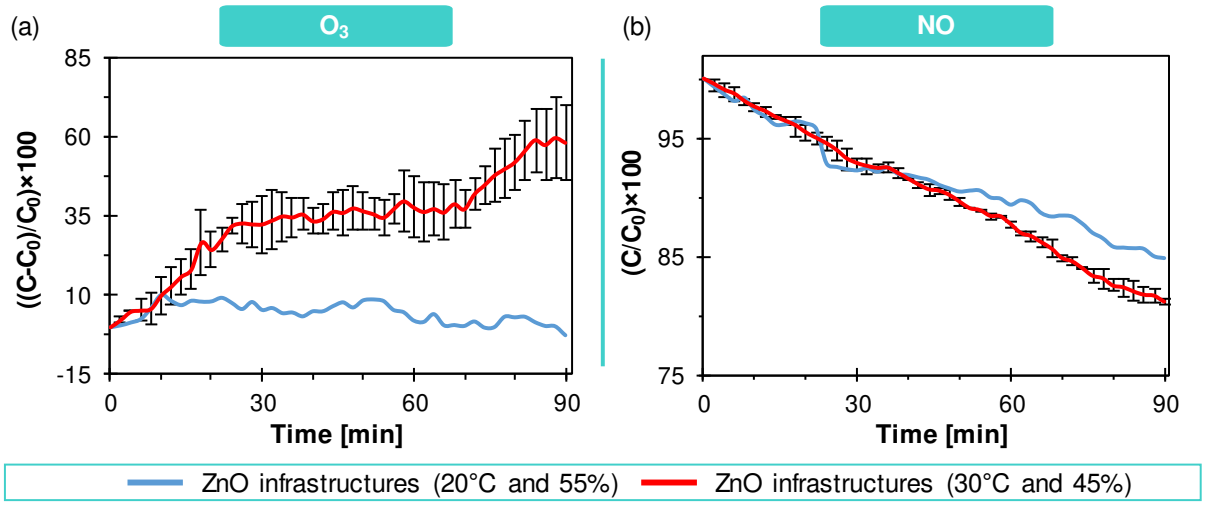

Figure 5. Pollutant evolution under solar light and different weather with ZnO (Plots of pollutant concentration evolution as function of photocatalysis time for ozone **(a)** and nitrogen monoxide **(b)** under artificial solar light with the presence of ZnO at different temperature and humidity conditions in Sense-City).

As it is possible to see on Figures 5(a) and 5(b), O_3 and NO follow different trends depending on climatic conditions. Temperature decrease and humidity increase are

beneficial for O_3 removal while it is not the case for NO. The electron-hole pairs are not created by heating but by light absorption, thus the temperature increase will not strongly affect the photocatalytic efficiency as shown in the literature (Chen and Chu, 2011; Herrmann, 1999). Therefore, it can be assumed that the relative humidity is the main factor affecting these results.

Water vapour may have positive impact on photocatalytic efficiency. In fact, water vapour augmentation could lead to more hydroxyl radical production and thus favour the synergic O_3 and VOCs degradation (equations (11) and (12)). Results are in agreement with the experiments done to prove the relative humidity increase leading to an enhancement of VOCs photodegradation (Nath et al., 2016; Bayjoo et al., 2017).

On the other side, water vapour could also have an adverse effect on pollutant photodegradation. Indeed, even if a higher water vapour concentration could favour hydroxyl radicals' formation; it could also simultaneously inhibit pollutant adsorption and degradation (Nath et al., 2016). Depending on the considered pollutants and their photodegradation pathway, the optimum relative humidity value will be different, which can justify the two different trends observed. In fact, literature suggests that high relative humidity has an adverse effect on NO removal by having strong adsorption competition onto the photocatalyst (Maggos et al., 2007; Wang et al., 2017; Bica and Staub, 2020). Besides, D. He *et al.* (2017) research study on carbon-wrapped and doped TiO_2 suggested that NO may prefer to react with $O_2^{\bullet-}$ and h^+ than with $OH^\bullet$. Thus, the addition of water would not necessarily be beneficial, insofar as hydroxyl radicals resulting from the water photo-oxidation would not be necessary for the NO photocatalytic degradation. For that reason,

even if the NO evolution is consistent with the T°C evolution, the RH may be the main factor affecting the photodegradation rate evolution.

In order to confirm that the RH is the key factor explaining both trends observed, new experiments at T = 20°C ~ 24°C with RH = 35% ± 3 % or RH = 55% ± 3 % were carried out. During this new measurement campaign, larger surfaces were deployed (Figure 2(c)) with three wall panels instead of two and 2 m^2 instead of 1 m^2 of bitumen road; and ventilation was stopped, in order to better understand what happens on the road surface. A VOCs sensor was also added in this new measurement campaign, to study the correlation between VOCs and O_3 photodegradation. Surprisingly, during this second campaign, the O_3 formation rate increased with the use of photocatalytic road infrastructures (Figures 6(a, b)). These unexpected results seem to confirm the strong Chapman cycle modification caused by VOCs from the car exhaust but also from the bitumen road. Therefore, the functionalized bitumen road may be responsible of the O_3 augmentation under solar light. To verify this last hypothesis, a small slab with only bitumen was exposed under sunlight (Figure 6(c)). As Figure 6(d) showed, O_3 formation was indeed recorded with the slab bitumen exposition under solar light. This result is coherent with recent literature results, which assume bitumen road produce secondary organic aerosol under solar exposure (Khare et al., 2020). The gap between the results with and without ZnO demonstrated a lowest O_3 formation in humid conditions (RH = 55%).

In humid conditions, at RH = 55%, the VOCs photodegradation is recorded, which is not the case at RH = 35% (Figures 6(e, f)). A better photodegradation rate could probably be obtained by taking the measurements near the road surface and with a more sensitive sensor. Nevertheless, as it can be seen on Figures 6(a) and 6(e), a correlation between VOCs

and O_3 evolution was observed with a better degradation at higher humidity level. These results confirm, first, the Chapman cycle modification by VOCs from bitumen road; second, that relative humidity is the key factor explaining the previous results. This last point was also demonstrated by results on NO pollutant, where a better photodegradation was obtained at RH = 35% (Figures 6(g, h)).

To conclude, environmental conditions will have different impacts on different pollutants photocatalytic degradation, the more important one being relative humidity. Consequently, photocatalytic road infrastructure efficiency will vary depending on pollutants and climatic conditions (Chen and Chu, 2011). Moreover, ventilation shutdown in Sense-City led to a slight decrease of the efficiency. Thus, photocatalytic efficiency may be subject to wind, road traffic and urban planning (Demeestere et al., 2008). In fact, a reasonable airflow rate will improve the depollution rate. Nevertheless, a high flow rate may have an adverse effect by reducing the time contact between pollutant molecules and photocatalyst (Staub de Melo and Trichês, 2012; Sleiman et al., 2009).

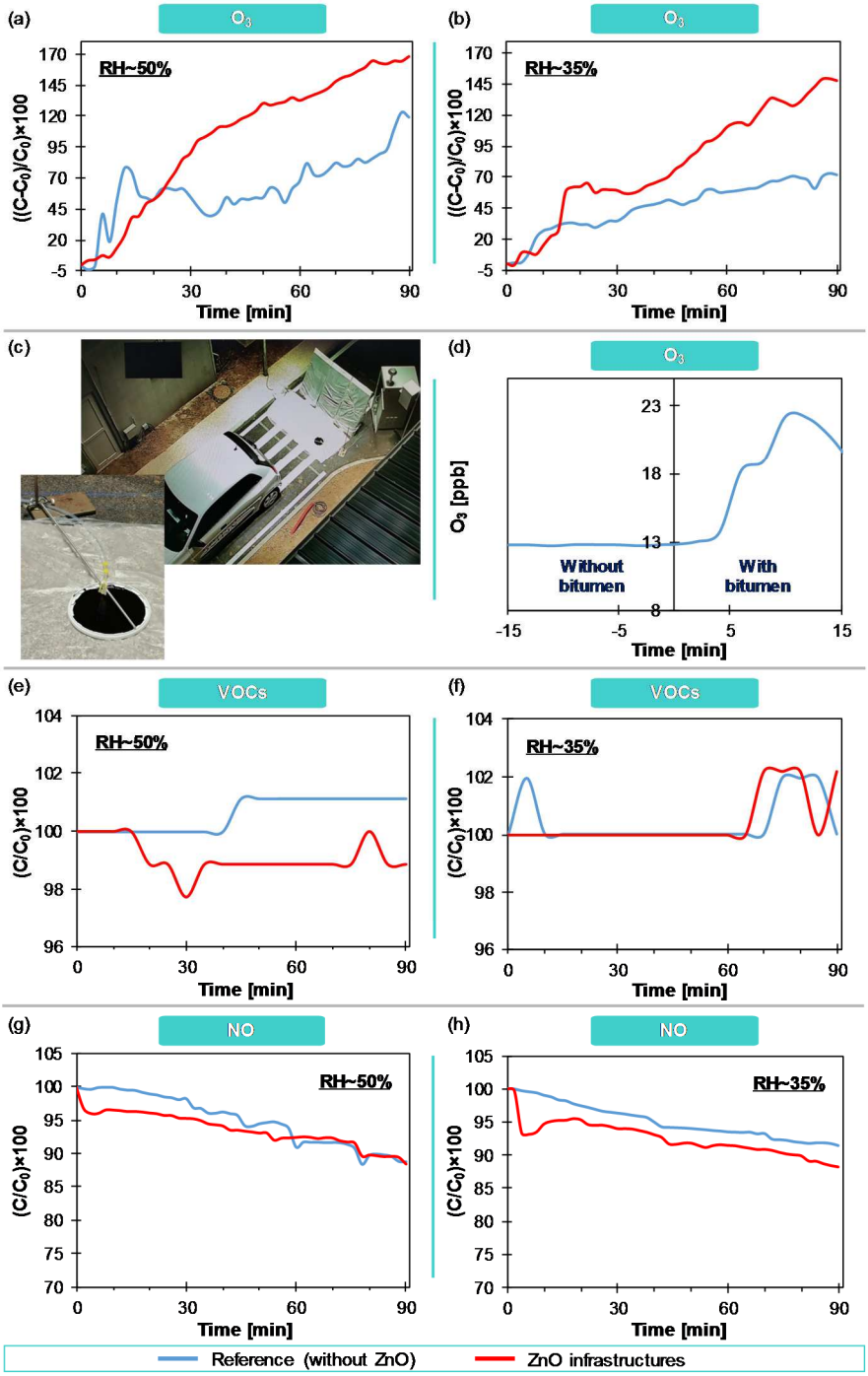

Figure 6. Pollutant evolution under solar light and different relative humidity percentage with ZnO (Plots of ozone concentration evolution as function of time under artificial solar light phase with and without the presence of ZnO at different humidity conditions **(a, b)**; Pictures of experimental set-up for floor tile bitumen emission investigation **(c)**; Plots of ozone concentration evolution as function of time under artificial solar light with the presence of bitumen slab **(d)**; Plots of volatile organic compounds **(d, e)** and nitrogen monoxide **(g, h)** concentration evolution as function of time under artificial solar light phase with and without the presence of ZnO at different humidity conditions).

3.2.3 Track type and distance from the road influences onto photocatalytic efficiency

Bitumen roads are known to be responsible of VOCs emission (Khare et al., 2020) and thus could increase O_3 emissions, as measured in Sense-City (Figure 6(a-d)). Hence, experiments with only 3 tiling wall panels as paved road were carried out at T = 30°C ± 3°C and RH = 30% ± 4% (Figure 2(d)). Ventilation remains shutdown. Influence of distance between ZnO surface and analyser was also studied in this part by placing it 50 cm above the tiling surface (Figure 2(e)).

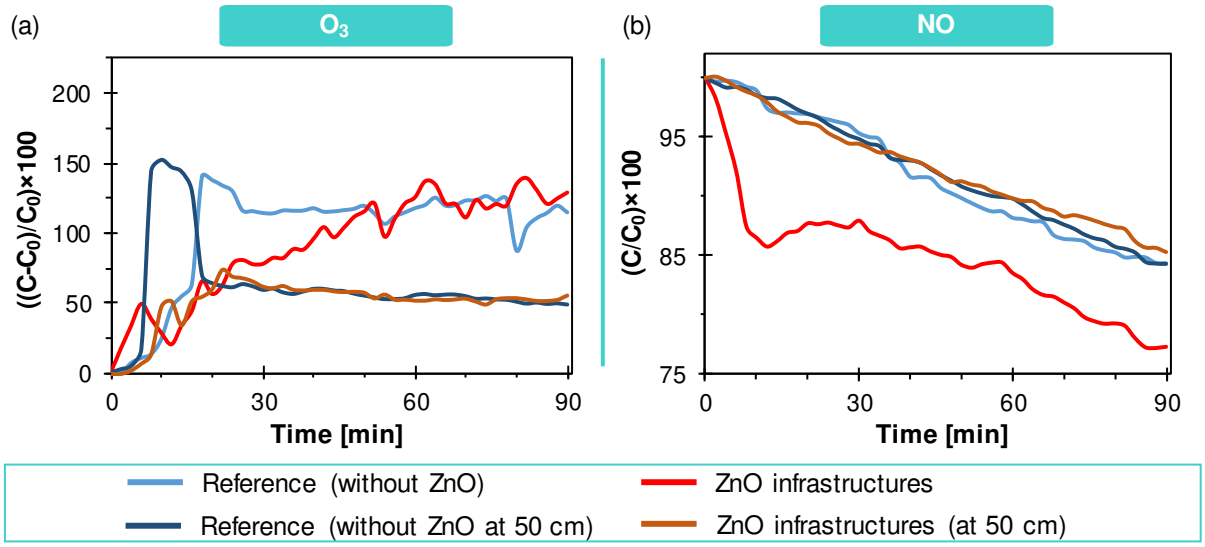

Figure 7. Pollutant evolution under solar light and at different distances from ZnO surface (Plots of pollutants concentration evolution as function of time for ozone **(a)** and nitrogen monoxide **(b)** with and without the presence of ZnO at different distance from the photocatalyst surface).

In accordance with the data reported in previous parts, tiling-paved roads showed a good photocatalytic efficiency and followed the same depollution trends with ventilation on, when the influence of bitumen road is negligible (Figures 7(a, b)). The photocatalytic paved road led therefore to less pollution emissions than bitumen road, and thus is more competitive for car exhaust depollution. Results with analysers 50 cm above the ZnO surface did not allow to record photocatalytic activity in the absence of ventilation (Figures 7(a, b)).

It is therefore possible to assume that the previous results without ventilation may be more representative of how functionalized bitumen roads would behave in real atmospheric conditions.

4. Conclusion

In this work, a scale-up of ZnO nanostructure synthesis on construction materials, such as tiling and rock aggregates, successfully provided 2 × 1 m² of functionalized bitumen road and 3 × 0.63 m² of functionalized tiling which can be used as walls and/or paved roads with an excellent ZnO nanostructures homogeneity. Then, functionalized paved roads and bitumen roads demonstrated a promising photocatalytic activity for real car exhaust pollutants purification at large scale in a climatic chamber (Sense-City). All car exhaust components studied, such as O_3, CO_X, COVs and NO_X, showed a downward trend in presence of ZnO surfaces. With the use of photocatalytic road infrastructures, O_3 and CO emissions under natural sunlight were divided at most by 2 and 4.8, respectively. Slight improvement of CO_2 and NO reductions were also recorded with a reduction by 1.09. Therefore, photocatalytic road infrastructures proved their very competitive performance for simultaneous removal of the car exhaust pollutants. Different experimental conditions were tested and the results showed that depending on pollutants, the weather conditions had varying influence. Trend modifications were mainly attributed to relative humidity. Increasing the relative humidity leads to better O_3 and VOCs depollution, but also to a worse purification of NO. Conversely, better NO degradation was obtained by decreasing the relative humidity to the detriment of O_3 and VOCs depollution. At this scale, without air ventilation, the photocatalytic depollution seems to be less efficient, and no photocatalytic activity was detected far away from the photocatalyst surface (50 cm above the

photocatalyst surface). Air ventilation shut down during experiment seems to demonstrate that bitumen roads could play a part in pollutant emission under sunlight.

Although purification results were less good than those obtained at laboratory scale, experiments at large scale in Sense-City with a real complex pollutants source may be more realistic for a transposition to real life applications as the next generation of depolluting road and are rather promising. Besides, observations provide insights into understanding the pollutants evolution and the synergies between the degradation of the different molecules. Many studies are still needed for a better understanding, such as surveys on the influence of road traffic airflow, road track type, of the abrasion of climate, and of the sunlight variations on the photocatalysis efficiency. Nevertheless, these results are very promising with no loss of efficiency during all experiment campaigns even after one year of storage without any special precautions.

Acknowledgements

This study was funded by the "I-Street" project (2017, ADEME via the Investissements d'Avenir Program, France) with a close collaboration with Eiffage (Dr. Flavien GEISLER and Dr Simon POUGET) and IFSTTAR (Dr. Nicolas Hautière). Data analysis work was supported by the Smart Lab LABILITY of the University Gustave Eiffel, funded by the Région Île de France under Grant N° 20012741.

The financial and technical support linked to this project provided are gratefully acknowledged. The authors would like to thank to Florent Schrevel and Ludovic Longin from Eiffage for their technical help on the bitumen road realisation. The authors would like to thank Dr. Flavien GEISLER for his suggestion to use cold bitumen emulsion. The authors would like to thank to Eric Dimnet, Anne Ruas, Stephane Butttigieg and Erick Merliot from Sense-City team (UGE) for invaluable help before and during campaign measurements in Sense-City. The authors would like to thank Nathan Martin from UGE for his invaluable help on this project.

Author Contributions

Marie Le Pivert: Synthetized and characterized samples, performed experiments in Sense-City during the both campaigns, Conceptualization, Writing – original draft, Investigation, Formal analysis, Validation, **Olivier Kerivel:** Synthetized and characterized samples, performed experiments in Sense-City during one campaign, Investigation, **Brahim Zerelli:** Synthetized and characterized samples, performed experiments in Sense-City during one campaign, Investigation, **Yamin Leprince-Wang:** Performed experiments in Sense-City during the both campaigns, Conceptualization, Supervision, Writing – review & editing, Project administration, Funding acquisition.

Competing interests

The authors declare no competing interests.

Reference:

[1] World Health Organization, 2016. Ambient air pollution: A global assessment of exposure and burden of disease. Geneva.

[2] Senff, L., Tobaldi, D.M., Lemes-Rachadel, P., Labrincha, J.A., Hotza, D, 2014. The influence of TiO_2 and ZnO powder mixtures on photocatalytic activity and rheological behaviour of cement pastes. Constr. Build. Mater. 65, 191–200. https://doi.org/10.1016/j.conbuildmat.2014.04.121.

[3] Singh, V.P., Sandeep, K., Kuswaha, H.S., Powar, S., Vaish, R., 2018. Photocatalytic, hydrophobic and antimicrobial characteristics of ZnO nano needle embedded cement composites. Constr. Build. Mater. 185, 285-294. https://doi.org/10.3389/fmicb.2018.00422.

[4] Hüsken, G., Hunger, M., Brouwers, H.J.H., 2009. Experimental study of photocatalytic concrete products for air purification. Build. Environ. 44, 1463-2474. https://doi.org/10.1016/j.buildenv.2009.04.010.

[5] Cerro-Prada, E., Garcia-Salgado, S., Quijano, M.A., Varela, F., 2018. Controlled Synthesis and Microstructural Properties of Sol-Gel TiO_2 Nanoparticles for Photocatalytic Cement Composites. Nanomaterials 9, 1-16. https://doi.org/10.3390/nano9010026.

[6] Guo, M.Z., Ling, T.C., Poon, C. S., 2017. Photocatalytic NO_X degradation of concrete surface layers intermixed and spray-coated with nano-TiO_2: Influence Of experimental factors. Cem. Concr. Compos. 83, 279-289. https://doi.org/10.1016/j.cemconcomp.2017.07.022.

[7] Nath, R.K., Zain, M.F.M., Jamil, M., 2016. An environment-friendly solution for indoor air purification by using renewable photocatalyst in concrete: A review. *Renew.* Sust. Energ. Rev. 62, 1184-1194. https://doi.org/10.1016/j.rser.2016.05.018.

[8] Darvish, S.M., Ali, A.M., Sani, S.R., 2020. Designed air purifier reactor for photocatalytic degradation of CO_2 and NO_2 gases using MWCNT/TiO_2 thin films under visible light irradiation. Mater. Chem. Phys. 248, 122872. https://doi.org/10.1016/j.matchemphys.2020.122872.

[9] Grande, F., Tucci, P., 2016. Titanium dioxide nanoparticles: a risk for human health? Mini Rev. Med. Chem. 16, 762-769. https://doi.org/10.2174/1389557516666160321114341.

[10] Dar, G.I., Saeed, M., Wu, A., 2020. TiO_2 Nanoparticles: Application in Nanobiotechnology and Nanomedicine, in: Wu, A., Ren, W. (Eds.), Toxicity of TiO_2 Nanoparticles. Wiley-VCH, Weinheim. https://doi.org/10.1002/9783527825431.ch2.

[11] Liu, J., Wang, P., Qu, W., Li, H., Shi, L., Zhang, D., 2019. Nanodiamond-decorated ZnO catalyst with enhanced photocorrosion-resistance for photocatalytic degradation of gaseous toluene. Appl. Catal. B 157, 117880. https://doi.org/10.1016/j.apcatb.2019.117880.

[12] Shinde, R., Tambade, P.S., Chaskar, M.G., Gadave, K.M., 2017. Photocatalytic degradation of dyes in water by analytical reagent grades ZnO, TiO_2 and SnO_2: a comparative study. Drink. Water Eng. Sci. 10, 109-117. https://doi.org/10.5194/dwes-10-109-2017.

[13] Pastor, A., Balbuena, J., Cruz-Yusta, M., Pavlovic, I., Sánchez, L., 2019. ZnO on rice husk: A sustainable photocatalyst for urban air purification. Chem. Eng. J. 368, 659-667. https://doi.org/10.1016/j.cej.2019.03.012.

[14] Li, Z., Yang, R., Yu, M., Bai, F., Li, C., Wang, Z.L., 2008. Cellular Level Biocompatibility and Biosafety of ZnO Nanowires. J. Phys. Chem. C 112, 20114-20117. https://doi.org/10.1021/jp808878p.

[15] Wang, C.F., Tzeng, F.S., Chen, H.G., Chang, C.H., 2012. Ultraviolet-durable superhydrophobic zinc oxide-coated mesh films for surface and underwater-oil capture and transportation. Langmuir 28, 10015-10019. https://doi.org/10.1021/la301839a.

[16] Zhang, Y., Huang, X., Yeom, J., 2019. A Floatable Piezo-Photocatalytic Platform Based on Semi-Embedded ZnO Nanowire Array for High-Performance Water Decontamination. Nanomicro. Lett. 11, 1-14. https://doi.org/10.1007/s40820-019-0241-9.

[17] Danwittayakul, S., Jaisai, M., Koottatep, T., Dutta, J., 2013. Enhancement of Photocatalytic Degradation of Methyl Orange by Supported Zinc Oxide Nanorods/Zinc Stannate (ZnO/ZTO) on Porous Substrates. Ind. Eng. Chem. Res. 52, 13629-13636. https://doi.org/10.1021/ie4019726.

[18] Le Pivert, M., Poupart, R., Capochichi-Gnambodoe, M., Martin, N., Leprince-Wang, Y., 2019. Direct Growth of ZnO Nanowires on Civil Engineering Materials: Smart Materials for Supported Photodegradation. Microsyst. Nanoeng. 5, 57. https://doi.org/10.1038/s41378-019-0102-1.

[19] Le Pivert, M., Zerelli, B., Martin, N., Capochichi-Gnambodoe, M., Leprince-Wang, Y., 2020. Smart ZnO decorated optimized engineering materials for water purification under natural sunlight. Constr. Build. Mater. 257, 119592. https://doi.org/10.1016/j.conbuildmat.2020.119592.

[20] Maggos, T., Bartzis, J.G., Liakou, M., Gobin, C., 2007. Photocatalysis degradation of NOx gases using TiO_2-containing paint: A real scale study. J. Hazard. Mater. 146, 668-673. https://doi.org/10.1016/j.jhazamat.2007.04.079.

[21] Chen, M., Chu, J.W., 2011. NOx photocatalytic degradation on active concrete road surface – from experiment to real-scale application. J. cleaner Prod. 19, 1266-1272. https://doi.org/10.1016/j.jclepro.2011.03.001.

[22] Sense-City. https://sense-city.ifsttar.fr/en/ (accessed 08 March 2021).

[23] Chevalier-César, C., Capochichi-Gnambodoe, M., Leprince-Wang, Y. 2014. Growth mechanism studies of ZnO nanowire arrays via hydrothermal method. App. Phys. A 115, 953-960. https://doi.org/10.1007/s00339-013-7908-8.

[24] Wang, D., Leng, Z., Yu, H., Hüben, M., Kollmann, J., Oeser, M., 2017. Durability of epoxy-bonded TiO_2 modified aggregate as a photocatalytic coating layer for asphalt pavement under vehicle tire polishing. Wear 382-383, 1-7. https://doi.org/10.1016/j.wear.2017.04.004 .

[25] Cui, S., Li, R. Pei, J., Wen, Y., Li, Y., Xing, X., 2020. Automobile exhaust purification over g-C3N4 catalyst material. Materials Chemistry and Physics 247, 122867. https://doi.org/10.1016/j.matchemphys.2020.122867.

[26] Liu, J., Li, Y., Li, Z., Ke, J., Xiao, H., Hou, Y. 2018. In situ growing of $Bi/Bi_2O_2CO_3$ on Bi_2WO_6 nanosheets for improved photocatalytic performance. Catal. Tod., 314, 2-9. https://doi.org/doi:10.1016/jcattod.2017.12.001.

[27] Da Costa Filho, B.M., Silva, G.V, Boaventura R. A.R., Dias, M.M., Lopes, J.C.B., Vilar, V.J.P., 2019. Ozonation and ozone-enhanced photocatalysis for VOC removal from air streams: Process optimization, synergy and mechanism assessment. Sci. of the Tot. Environ. 387, 1357-1368 (2019). https://doi.org/10.1016/j.scitotenv.2019.05.365.

[28] Bayjoo, y., Sun, H., Liu, J., Pareek, V. K., Wang, S, 2017. A review on photocatalysis for air treatment: from catalyst development to reactor design. Chem. Eng. J. 310, 537-559. https://doi.org/10.1016/j.cej.2016.06.090.

[29] Kowsari, E., Bazri, B., 2014. Synthesis of rose-like ZnO hierarchical nanostructures in the presence of ionic liquid_Mg^{2+} for air purification and their shape-dependent photodegradation of SO_2, NO_X, and CO. Appl. Cata., A 475, 325-334. http://doi.org/10.1016/j.apcata.2014.01.046.

[30] Todorova, N., Giannakopoulou T., Pomoni, K., Yu, J., Vaimakis, T., Trapalis, C., 2015. Photocatalytic NOx oxidation over modified ZnO/TiO_2 thin films. Catal.Today 252, 41-46. https://doi.org/10.1016/j.cattod.2014.11.008.

[31] He, D., Li, Y., Wang, I., Wu, J., Yang, Y., An, Q., 2017. Carbon wrapped and doped TiO_2 mesoporous nanostructure with efficient visible-light photocatalysis for NO removal. App. Surf. Sci. 391, 318-325. http://doi.org/10.1016/j.apsusc.2016.06.186.

[32] Mahy, J. G., Carlos, A.P., Hollevoet, J., Courard, L., Boonen, E., Lambert, S.D., 2019. Durable photocatalytic thin coating for road applications. Constr. and build. mater. 215, 422-434. https://doi.org/10.1016/j.conbuildmat.2019.04.222.

[33] Staub de Melo, J. V., Trichês, G., 2012. Evaluation of influence of environmental conditions on the efficiency of photocatalytic coatings in the degradation of nitrogen oxides (NOx). Build. and Environ. 49, 117-123. https://doi.org/10.1016/j.buildenv.2011.09.016.

[34] Herrmann, J.M., 1999. Heterogeneous photocatalysis: fundamentals and applications to removal of various types of aqueous pollutants. *Catal. Today* 53, 115-129. https://doi.org/10.1016/S0920-5861(99)00107-8.

[35] Bica, B. O., Staub, J. V., 2020. Concrete blocks nano-modified with zinc oxide (ZnO) for photocatalytic paving: Performance comparison with titanium dioxide (TiO_2). Constr. Build. Mater. 252, 119120. https://doi.org/10.1016/j.conbuildmat.2020.119120.

[36] Khare, P., Machesky, J., Soto, R., He, M., Presto, A.A., Gentner D.R., 2020. Asphalt-related emissions are a major missing non-traditional source of secondary organic aerosol precursors. Sci. Adv. 6, 1-14. https://doi.org/10.1126/sciadv.abb9785.

[37] Demeestere, K., Dewulf, J., De Witte, B., Beeldens, A. Van Langenhove, H., 2008. Heterogeneous photocatalytic removal of toluene from air on building materials enriched with TiO_2. Build. and Environ. 43, 406-414. https://doi.org./10.1016/j.buildenv.2007.01.016.

[38] Sleiman, M., Conchon, P., Ferronato, C., Chovelon, J. M., 2009. Photocatalytic oxidation of toluene at indoor air levels (ppbv): Towards a better assessment of conversion, reaction intermediates and mineralization. Appl. Catal., B. 86, 159-165. https://doi.org./doi:10.1016/j.apcatb.2008.08.003.

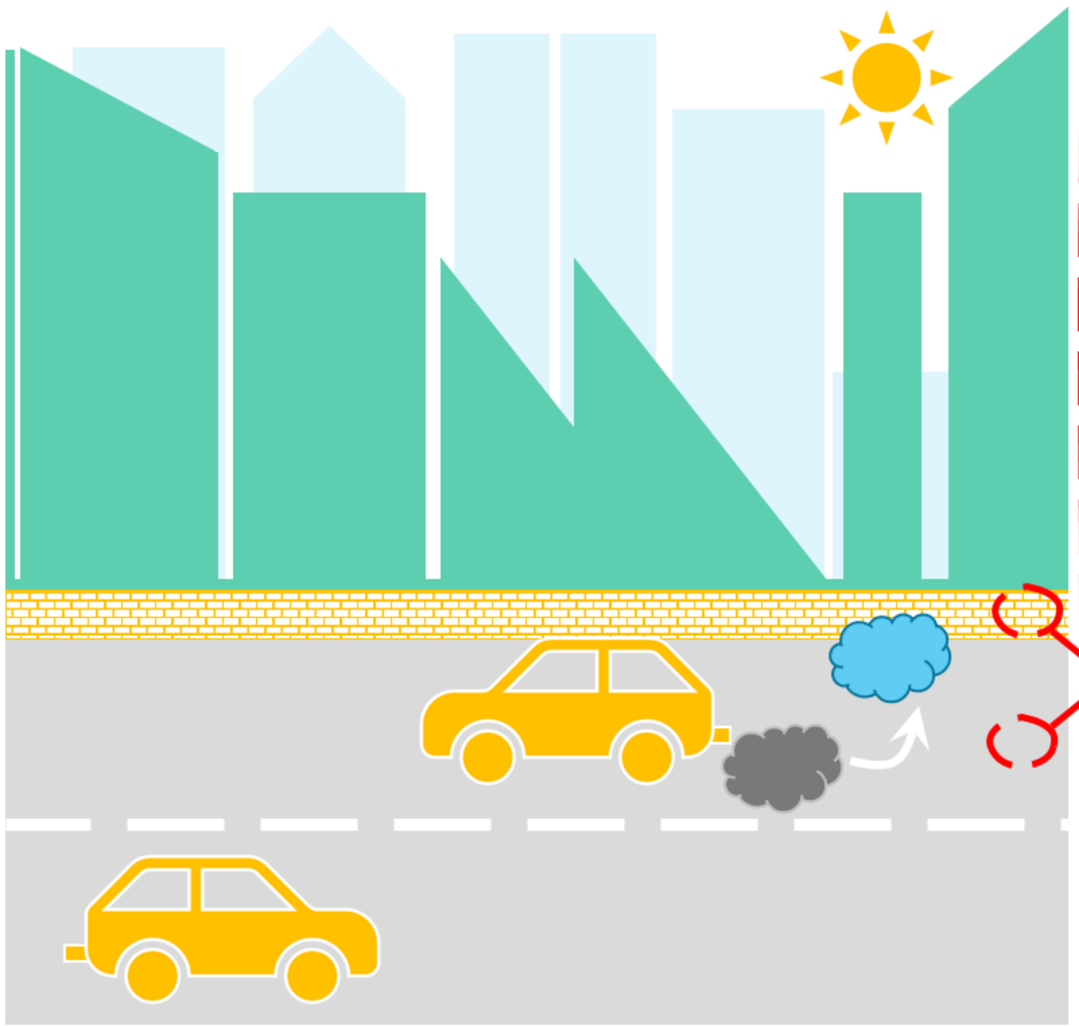

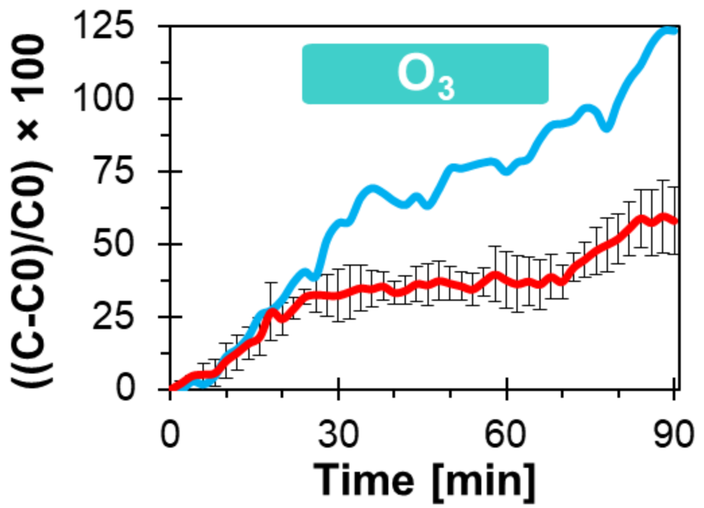

Reference (without ZnO)

ZnO infrastructures

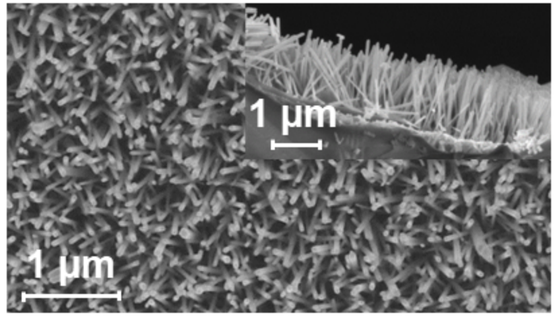

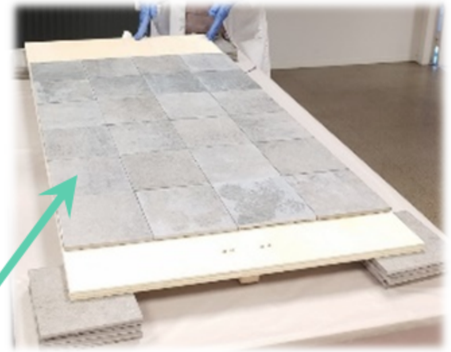

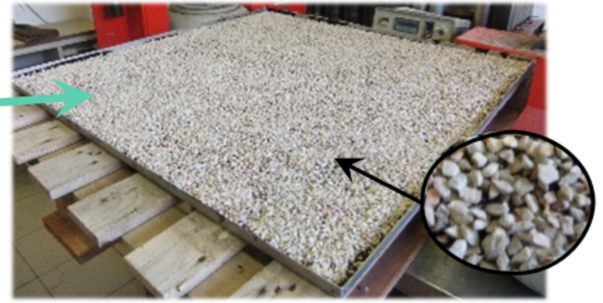

Road fonctionnalisation